Journal of Geointerface, Vol. 4, No. 2, December 2025, pp. 125–140 e-ISSN: 2583-6900

Axinite over tourmaline: A new perspective on boron pathfinders in the gold-bearing zones of Dongargarh-Kotri belt, Central India

Tushar Meshram [1,*], Nilashree Raychowdhury[1], Lovelesh Soni[1], Rajkumar Meshram[1], Girish Mayachar[2], Debjani Sarkar[2], Kamal Kannan D[3], Savita Chaurpagar[1], Rajesh Wasnik[1], M L Dora [4], Srinivasa R. Baswani[5], Purushottam Dhunde[1]

[1] *Geological Survey of India, Central Region, Nagpur, India*
[2] *Geological Survey of India, Central Head Quarter, Kolkata, India*
[3] *Geological Survey of India, Southern Region, Bangalore, India*
[4] *Jawaharlal Nehru University, New Delhi, India*
[5] *Geological Survey of India, Southern Region, Hyderabad, India*

ABSTRACT

Dongargarh-Kotri Belt (DKB) is a storehouse for gold occurrences and shows the potential concentration of gold (12 ppm to 37 ppm) with associated arsenopyrite-rich acid volcanics and BIF throughout the DKB. Boron is commonly associated with gold mineralisation, as suggested by the widespread occurrences of tourmaline in gold-bearing quartz veins worldwide. Axinite, a calc-silicate of boron, is rare and instead of tourmaline, at places associated with auriferous zones or base-metal deposits. We have reported the axinite associated with gold-sulphide-rich quartz veins along the interface of volcanic and sedimentary rocks of the DKB. The mineral chemistry shows high B_2O_3 8.03 avg. wt.%, FeO 8.99 avg. wt.%, with very low MnO and MgO (<0.5 wt.%) and classified it ferro-axinite. The formation of ferro-axinite suggests limited carbonatization, therefore available Ca combines with B, Fe, and Si in ferro-axinite and avoids the generation of tourmaline. The presence of pyrite, chalcopyrite, pyrrhotite, marcasite and the conversion of marcasite from pyrrhotite generally confirm high sulphidation, at 300 °C and low pH (<5).

The fluid inclusion and Raman studies revealed the presence of primary aqueous and CO_2 phases with low to moderate salinity and two ranges of the temperature of homogenization i.e, 150–200 °C and ~300 °C. The presence of axinite-quartz vein with associated sulphide and gold mineralisation within the boron-rich hydrothermal system along the brittle-ductile zones in the DKB suggested their low pressure, low to moderate salinity, low pH and ~300 °C temperature also suitable for precipitation of gold. The present study provides evidence of the spatiotemporal association of ferro-axinite with the sulphide gold mineralisation in the area as well as along the DKB may be used as an indicator mineral or pathfinder.

ARTICLE HISTORY

Received: 12 August 2025
Revised: 10 September 2025
Accepted: 11 September 2025

https://doi.org/10.5281/zenodo.17105426

KEYWORDS

Axinite
Tourmaline
Gold-Sulphide
Marcasite
Dongargarh-Kotri Belt

*Corresponding author. Email: tusharmeshram1984@gmail.com, tushar.meshram@gsi.gov.in (TM), nilasree.raychowdhury@gsi.gov.in (NR), lovelesh.soni@gsi.gov.in (LS), rr.meshram@gsi.gov.in (RM), girish.mayachar@gsi.gov.in (GM), debjani.sarkar@gsi.gov.in (DS), kamalakannan.d@gsi.gov.in (KKD), chaurpagar.nilkanth@gsi.gov.in (SC), rajesh.wasnik@gsi.gov.in (RW), dorageol@gmail.com (MLD), srinivasa.baswani@gsi.gov.in (SRB), dhunde.madhukarrao@gsi.gov.in (PD)

1. Introduction

The North-South trending Dongargarh-Kotri Belt (DKB) in Bastar Craton is an Early Proterozoic supracrustal sequence with imprints of repeated volcanic, plutonic and tectonic events which have rendered this belt most conducive to mineralisation (Ramachandra and Roy, 2012; Roy and Ramachandra, 2012; Mishra and Dutta, 2012; Saha et al., 2012). DKB is a volcano-sedimentary sequence represented by intrusive acid and basic volcanics and tuffaceous rock along with BIF, sandstone and conglomerate classified into the Dongargarh and Kotri Supergroups (Sarkar et al., 1981, 1994). The DKB represents an intracontinental rift-related sequence (Ghosh and Pillay, 2012; Neogi et al., 1996; Ramachandra and Roy, 1998; Krishnamurthy et al., 1990). The felsic volcanics constitute a primary source of economic-grade of gold mineralisation and several gold prospects along with old workings have been reported from the eastern, central and western parts of the DKB (Saha et al., 2012). The gold mineralisation in the DKB has spatial-temporal relationships with the felsic volcanic and associated brittle to brittle-ductile shear zones. These brittle to brittle-ductile shear zones provided the path for hydrothermal system to carry sulphide gold mineralisation within quartz veins along these shear zones (Saha et al., 2012; Mishra et al., 2012).

The axinite group comprised of ferro-axinite, mangan-axinite, magnesio-axinite and tinzenite with the general formula $(Ca,Mn)_4(Fe^{2+}, Mn, Mg)_2(Al,Fe^{3+})_4B_2Si_8O_{30}(OH)_2$ are common in various rocks characterized by high activity of Ca (Mn) and B, but low activity of Al (Pringle and Kawachi, 1980; Grew, 1996). It often forms in hydrothermal and contact-metamorphic environments that can also host tourmaline, another boron-rich silicate. In certain geological settings, such as pegmatites or alpine fissures, tourmaline may crystallize first from high-temperature, boron-rich fluids. As the physical and chemical conditions evolve (e.g., decreasing temperature, changing pH, or fluid salinity), axinite may later precipitate or replace tourmaline (Shcheka et al., 2023). For example, in the Dalnegorsk ore district (Russia), axinite formation has been linked to the interaction of retrograde boron-rich fluids with earlier skarn assemblages, indicating that axinite may derive from the breakdown or alteration of tourmaline in response to fluid evolution (Shcheka et al., 2023). This makes axinite a useful indicator mineral, as its presence can reflect specific pressure-temperature-fluid histories and help identify zones of boron metasomatism, especially in skarn and greisen systems (Kowal-Linka and Rychła, 2022, Hammarstrom and Zen, 1986).

Axinite holds significance in mineral exploration primarily as an indicator of specific hydrothermal conditions rather than as a direct pathfinder for gold or sulphide mineralisation. It commonly forms in contact-metamorphic and hydrothermal settings such as skarns, where high-temperature boron-bearing fluids interact with carbonate-rich rocks. These geological environments often overlap with those favorable for the deposition of sulphides and, in some cases, gold. Previous studies suggest that axinite is not a classic pathfinder mineral like arsenopyrite, pyrite, or stibnite which are more directly associated with gold and base metal mineralisation. Rather, it serves as a contextual or indirect pathfinder by pointing to evolved, boron-enriched hydrothermal systems capable of hosting valuable ore bodies (Shcheka et al., 2023; Hammarstrom and Zen, 1986). For example, in skarn systems, axinite is typically found in the retrograde alteration zones, where decreasing temperatures and evolving fluid chemistries result in the formation of minerals like axinite, datolite, or tourmaline. This mineralogical assemblage often coincides with or lies adjacent to zones of base-metal sulphide or even gold mineralisation (Kowal-Linka and Rychła, 2022). The presence of axinite can, therefore, help delineate zones of fluid flow and metasomatism, making it a valuable clue in reconstructing ore-forming environments. For instance, in the Dalnegorsk ore district in Russia, axinite occurs in association with retrograde boron metasomatism and is genetically linked to fluids capable of transporting and precipitating sulphide minerals, highlighting its role as a hydrothermal system tracer (Shcheka et al., 2023).

Although axinite does not substitute for geochemically mobile pathfinder elements or sulphide indicator minerals such as arsenopyrite, it complements them by providing insight into the temperature–fluid–pH evolution of the mineralizing system. When axinite is found alongside minerals like pyrite or tourmaline, it can reinforce the interpretation of a boron-rich, mineralizing hydrothermal event and guide further exploration targeting sulphide -rich or gold-bearing zones (Hammarstrom and Zen, 1986; Kowal-Linka and Rychła, 2022).

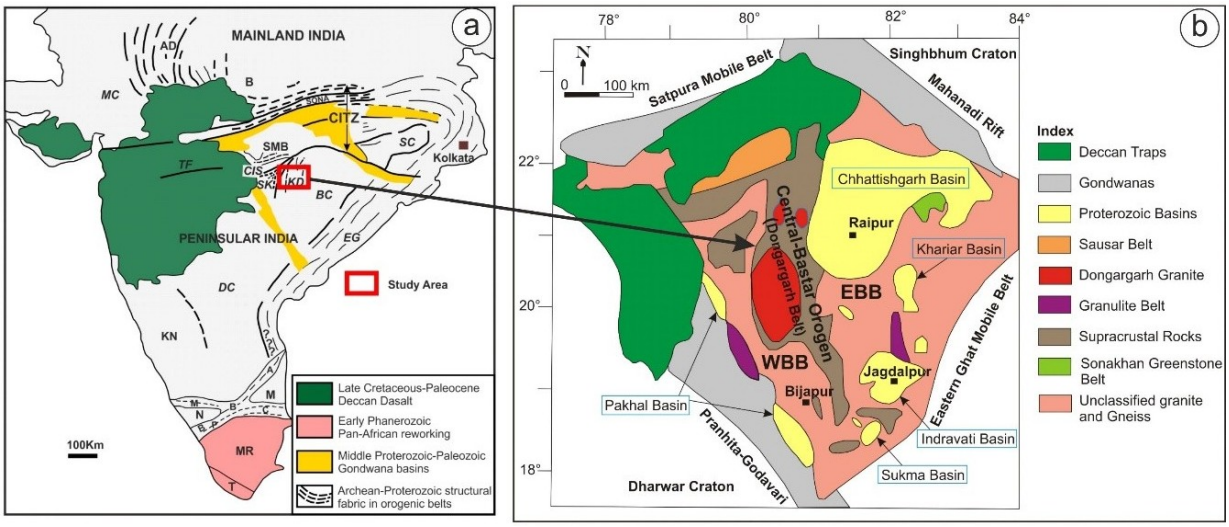

Fig. 1. a) Map of India showing regional tectonic domains and location of study area. b) Geological map of the Bastar craton showing Dongargarh Kotri belt (Central Bastar Orogen).

A number of occurrences of axinite have been reported worldwide (Andreozzi et al., 2004). However, so far, only the occurrence of axinite has been reported from the hydrothermal alteration zone of the Askot base metal mineralisation in the Kumaon Himalaya, India (Govil et al., 2021). A number of calc-silicate minerals, such as tourmaline and dumortierite, have been reported from nearby study areas in the Sakoli Fold Belt (Meshram and Ingle, 2012). However, the reporting of ferro-axinite in the volcanics of DKB is discussed for the first time (Table 1). The ferro-axinite is associated with quartz veins along the brittle to brittle-ductile shear zones passing through felsic volcanics, and also carries sulphide and gold mineralisation. Another occurrence is reported from the contact between the andesite and quartz pebble conglomerate/sandstone of the Bortalao Formation. In this paper, we present the mineralogy and petrographic features representing metallogenic stages and the major and trace element chemical data for ferro-axinite mineral and associated sulphide gold mineralisation from the area. We discuss the metallogenic conditions and evolution of the ore-forming fluids, with the ultimate aim of revealing the mineralogical processes to guide further exploration for targeting sulphide -rich or gold-bearing zones in DKB.

2. Regional Geology

The Bastar craton of central India is an important protocontinental nuclei of the global Archaean record (Bleeker, 2003; Naqvi, 2005). It is flanked by the ENE-WSW trending Central Indian Tectonic Zone (CITZ) towards the north, and is cross-cut by the N-S to NNE-SSW trending Kotri lineament that geographically corresponds to a collage of Archaean/Palaeoproterozoic supracrustal belts; collectively termed the Kotri-Dongargarh Mobile Belt (KDMB) (Fig. 1) (Ramakrishnan and Vaidyanadhan, 2010). It extends for approximately 250km, from about 40km south of Pratappur in the south to about 40km southwest of Amarkantak in the north, with an average width of 30km (Saha et al., 2012). The DKB is composed of acid-basic volcanics and a basic igneous suite of rocks, with admixtures of pyroclastics, agglomerates, and volcaniclastic sediments (Mishra and Dutta, 2012). The Dongargarh Supergroup is the younger volcano-sedimentary-granite belt of DKB, unconformably overlies the Sukma supracrustals, while its northern margin is tectonised along the Sausar Mobile Belt (Sarkar et al., 1981, 1994; Roy et al., 2000).

The Dongargarh Supergroup consists of two unconformable stratigraphic groups presumed to be of Proterozoic age: the Lower Nandgaon Group and Upper Khairagarh Group (Table 1). Each group is further subdivided into distinct volcano-sedimentary units. The Nandgaon Group comprises the Bijli rhyolite and the Pitapani basalt, which are tectonically associated with the surrounding Dongargarh granite (Deshpande et al., 1990). Bortalao Formation, a conglomerate/sandstone unit forms the basal part of the Khairagarh Group, which overlies the Pitapani

Journal of Geointerface, Vol. 4, No. 2, December 2025, pp. 125–140

e-ISSN: 2583-6900

Table 1. Representative electron probe analysis of the ferro-axinite from quartz-axinite veins of the Dongargharh-Kotri Belt.

DataSet/Point	213 / 1 .	214 / 1 .	217 / 1 .	218 / 1 .	224 / 1 .	225 / 1 .	226 / 1 .	228 / 1 .	229 / 1 .	230 / 1 .	125 / 1 .	126 / 1 .	127 / 1 .	128 / 1 .	130 / 1 .	
SiO_2	37.849	37.521	38.034	37.752	37.463	37.67	38.354	38.345	37.631	37.704	38.007	38.051	38.238	38.805	38.218	
TiO_2	0.2	0.031	0.055	0.291	0.194	0.15	0.139	0.094	0.075	0.375	0.802	0.159	0.416	0.105	0.15	
Al2O3	23.316	22.4	23.459	24.27	22.777	23.191	22.348	22.39	21.737	22.878	23.494	24.607	24.008	24.011	23.97	
FeO	9.478	10.246	8.463	9.076	9.524	9.622	10.887	9.552	9.722	9.322	7.755	7.88	8.016	7.882	7.512	
MnO	0.142	0.158	0.031	0.051	0	0	0.006	0.268	0.169	0.089	0.124	0.209	0	0	0.023	
MgO	0.045	0.197	0.024	0.035	0.004	0.008	0.027	0.409	0.091	0.033	0.063	0.001	0.072	0	0.04	
CaO	21.592	20.273	21.854	20.196	21.618	22.585	20.859	20.772	22.07	21.031	21.186	20.849	21.503	20.684	21.931	
Na2O	0.018	0	0.005	0	0	0.026	0	0.012	0	0.011	0	0.026	0	0.037	0.047	
K2O	0	0	0.002	0.014	0	0	0	0.01	0	0.065	0.029	0	0.014	0.039	0	
Calculation based on 32 (O,OH)																
																Avg.
B2O3	8.065	7.898	8.049	8.049	7.964	8.085	8.035	8.012	7.922	7.980	8.047	8.092	8.115	8.095	8.090	8.033147
SiO_2	37.849	37.521	38.034	37.752	37.463	37.670	38.354	38.345	37.631	37.704	38.007	38.051	38.238	38.805	38.218	37.97613
TiO_2	0.200	0.031	0.055	0.291	0.194	0.150	0.139	0.094	0.075	0.375	0.802	0.159	0.416	0.105	0.150	0.215733
Al2O3	23.316	22.400	23.459	24.270	22.777	23.191	22.348	22.390	21.737	22.878	23.494	24.607	24.008	24.011	23.970	23.25707
FeO	9.478	10.246	8.463	9.076	9.524	9.622	10.887	9.552	9.722	9.322	7.755	7.880	8.016	7.882	7.512	8.9958
MnO	0.142	0.158	0.031	0.051	0.000	0.000	0.006	0.268	0.169	0.089	0.124	0.209	0.000	0.000	0.023	0.084667
MgO	0.045	0.197	0.024	0.035	0.004	0.008	0.027	0.409	0.091	0.033	0.063	0.001	0.072	0.000	0.040	0.069933
CaO	21.592	20.273	21.854	20.196	21.618	22.585	20.859	20.772	22.070	21.031	21.186	20.849	21.503	20.684	21.931	21.26687
Na2O	0.018	0.000	0.005	0.000	0.000	0.026	0.000	0.012	0.000	0.011	0.000	0.026	0.000	0.037	0.047	0.012133
K2O	0.000	0.000	0.002	0.014	0.000	0.000	0.000	0.010	0.000	0.065	0.029	0.000	0.014	0.039	0.000	0.011533
TOTAL	100.705	98.724	99.976	99.734	99.544	101.337	100.655	99.864	99.417	99.488	99.507	99.874	100.382	99.658	99.981	99.92301
B	2.505	2.453	2.499	2.499	2.473	2.511	2.495	2.488	2.460	2.478	2.499	2.513	2.520	2.514	2.512	
Si	7.152	7.240	7.201	7.148	7.169	7.100	7.274	7.293	7.238	7.200	7.197	7.166	7.181	7.305	7.199	
Ti	0.028	0.004	0.008	0.041	0.028	0.021	0.020	0.013	0.011	0.054	0.114	0.023	0.059	0.015	0.021	
Al	5.192	5.094	5.234	5.415	5.136	5.152	4.995	5.019	4.927	5.149	5.243	5.461	5.313	5.327	5.321	
Fe(ii)	1.497	1.653	1.340	1.437	1.524	1.517	1.727	1.519	1.564	1.488	1.228	1.241	1.259	1.241	1.183	
Mn	0.023	0.026	0.005	0.008	0.000	0.000	0.001	0.043	0.028	0.014	0.020	0.033	0.000	0.000	0.004	
Mg	0.013	0.057	0.007	0.010	0.001	0.002	0.008	0.116	0.026	0.009	0.018	0.000	0.020	0.000	0.011	
Ca	4.371	4.191	4.433	4.097	4.432	4.561	4.238	4.232	4.548	4.302	4.298	4.206	4.326	4.172	4.426	
Na	0.007	0.000	0.002	0.000	0.000	0.010	0.000	0.004	0.000	0.004	0.000	0.009	0.000	0.014	0.017	
K	0.000	0.000	0.000	0.003	0.000	0.000	0.000	0.002	0.000	0.016	0.007	0.000	0.003	0.009	0.000	
TOTAL	20.787	20.717	20.729	20.659	20.763	20.873	20.758	20.731	20.802	20.715	20.624	20.653	20.681	20.596	20.695	

*Calculated from stoichiometry.

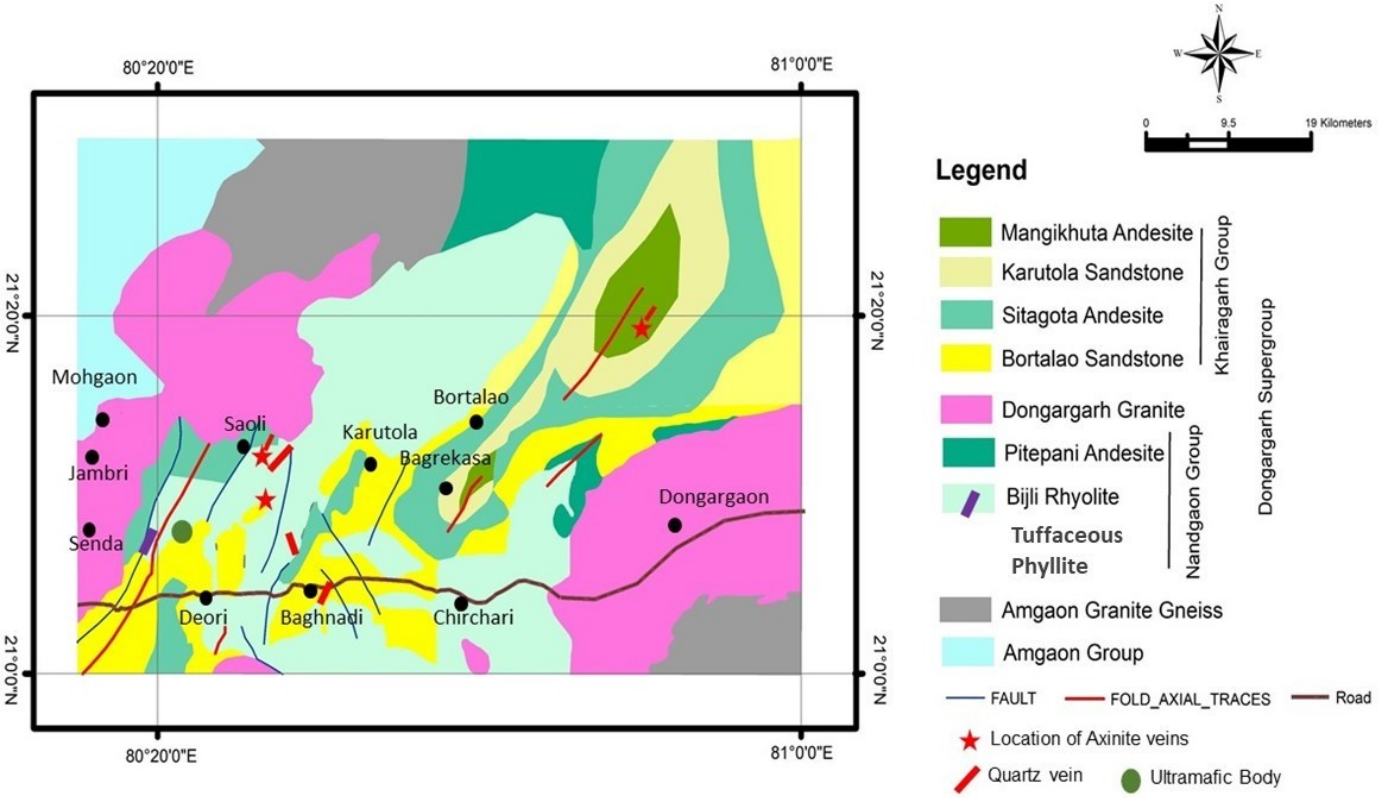

Fig. 2. Geological map of the central part of Dongargarh-Kotri Belt showing the location of gold-sulphide bearing quartz-axinite veins.

basalts and Bijli rhyolite. The Khairagarh Group consists of Sitagota, Mangikhuta and Kotima basalt formations that are alternately intercalated with the Karutola Formation quartz arenites and Ghogra Formation sub-arkosic arenites, respectively (Fig. 2).

The Dongargarh sequence is weakly deformed, forming the regional 'Sitagota Syncline' (Fig. 2) and has undergone low green schist facies metamorphism. Structural disposition of the units suggests the Bijli rhyolite to be the oldest unit, and the Mangikhuta volcanics to be the youngest (Sarkar et al., 1981, 1994; Sensarma and Mukhopadhyay, 2003). The present study area is situated in the central part of DKB and in the vicinity of the Sitagota Syncline. The crisscross venations occur along the brittle to brittle-ductile zones, show intense hydrothermal activity with the development of alteration mineralogy, i.e, epidote, chlorite, and axinite (Fig. 3a–b). Veins are occurring few centimeters to few meters long but axinite only restricted to the small veins (Fig. 3c), which are spatially and temporally associated with copper-gold mineralized hydrothermal system represented by smoky quartz veins in the area (Fig. 3d). Whereas, associated copper-gold mineralized veins have an extension upto 300m length and 10m to 15m width show smoky nature and contain fine dissemination of sulphide mineralisation with profuse chlorite and potassic alteration. The occurrences of axinite-quartz veins are reported from the contact zone between Sitagota andesite, Bijli rhyolite and Bartalao conglomerate/sandstone. Axinite generally occurs within Bijli rhyolite; specimens of a few centimeters in size show a violet to pink colour, occurring in association with quartz and epidote.

3. Methodology

Detailed silicate/ore petrographic studies of the axinite-quartz vein and associated sulphide minerals have been carried out using a Lieca DMRX-600 Model microscope equipped with a camera for photomicrographs at the Regional Petrology Laboratory, GSI, CR, Nagpur. Mineral phases were identified using a standard petrological microscope under transmitted light. They reflected light, followed by observations in a Carl Zeiss-EVO 40 Scanning Electron Microscope coupled with an Energy Dispersive Spectrometer at 20 kV and 63eV detector resolutions at

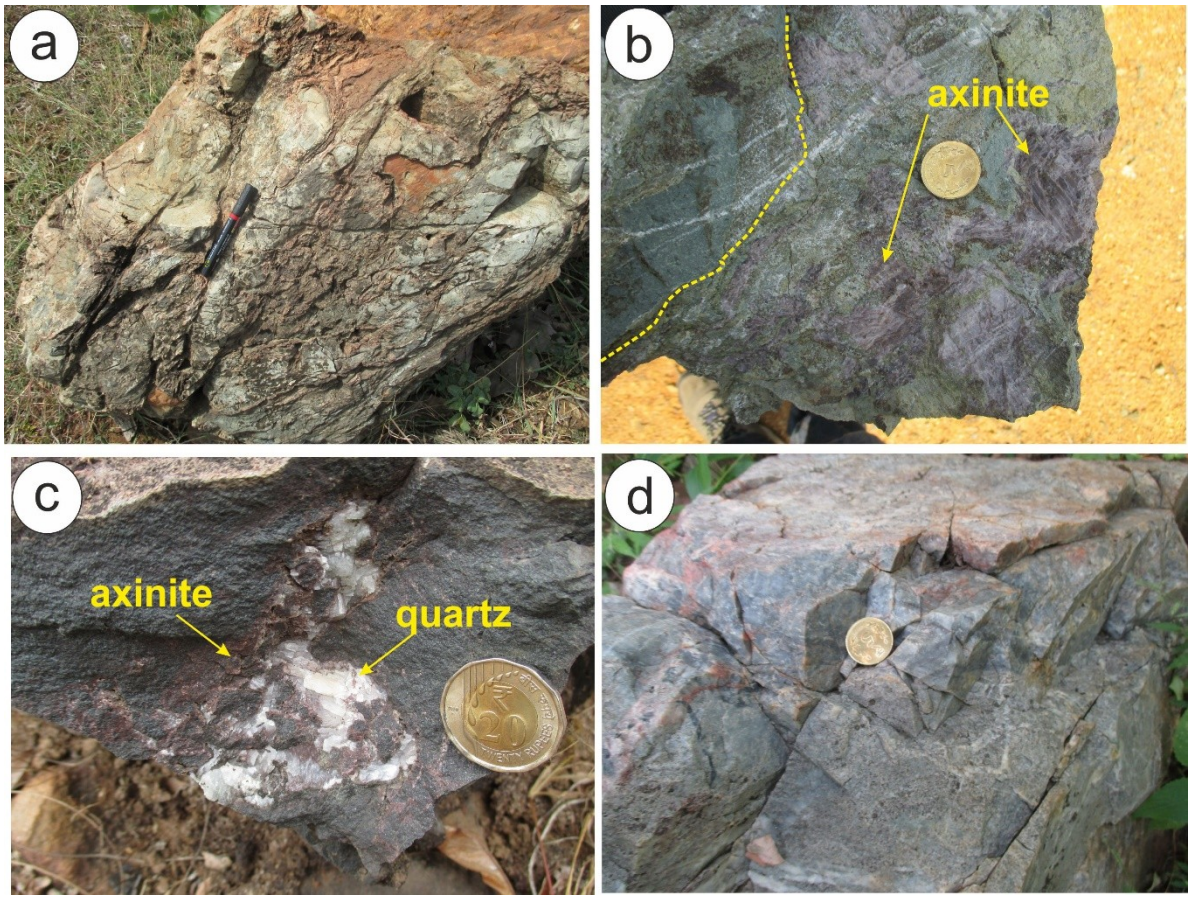

Fig. 3. a) Field photograph showing silicified rhyolite with network of axinite-quartz veins. b) close view of altered rhyolite with presence of purple-pink axinite-quartz veins c) close view of brownish-pink axinite-quartz vein along sandstone rhyolite contact. d) close view of smoky quartz vein contains sulphide and gold mineralisation.

the Geological Survey of India (GSI), Nagpur, India.

Silicate mineral phases were analysed using a CAMECA SX-100 Electron Microprobe Analyser (EPMA) equipped with five wavelength dispersive spectrometers (WDS) at the EPMA laboratories of the Geological Survey of India at Hyderabad. Calibration, overlap correction, and quantifications were performed with the CAMECA SX-100 Peak Sight-Geo Quanta software package. The silicate phases were analysed using 15 kV acceleration voltage and 15 nA beam current with 1 m beam diameter. The signals used are Si Ka, Na Ka, P Ka, K Ka, TiKa, CaKa, Cr Ka, Fe Ka, Mn Ka, Ni Ka, Ba La, V Ka, Mg Ka, Al Ka, Zn Ka, Zr La for calibration of elements using natural standards for Na, Si, Ca, K, Fe, Mg, Mn, P, Zn, Zr, Ba, synthetic standards for Al, Ti, Cr and 100% metal standards for Ni and V. Standards used are jadeite for Na, wollastonite for Si, Ca, olivine for Mg, corundum for Al, orthoclase for K, rutile for Ti, chromite for Cr, haematite for Fe and rhodonite for Mn, barite for Ba, apatite for P, zircon for Zr, sphalerite for Zn. The counting time for peak measurement 10s, and half of the peak measurement time is allotted for background measurement. The precisions of the analyses are ±0.5% element concentrations. The ZAF matrix corrections were carried out using the CAMECA-supplied Peak Sight program (Pouchou and Pichoir, 1984). Representative samples from the alteration zone and axinite-quartz vein were selected to classification under the X-ray diffraction method at Mineral Physics Division, GSI, CR, Nagpur. The identified minerals, along with their spectra and wavelengths, are described in detail under the 'Results' section.

Axinite-quartz wafers were prepared at the Regional Petrology Division, GSI, Nagpur for Fluid inclusion by Laser Raman Spectroscopy study. Raman spectroscopy (Renishaw System 1000) was used to analyze the volatiles, gases, and fluids enclosed within the FIs at the GSI, Kolkata. An Ar ion laser with a wavelength of 514.5 nm and a 5 mWat 100% source power was used for the analyses. The spectral range

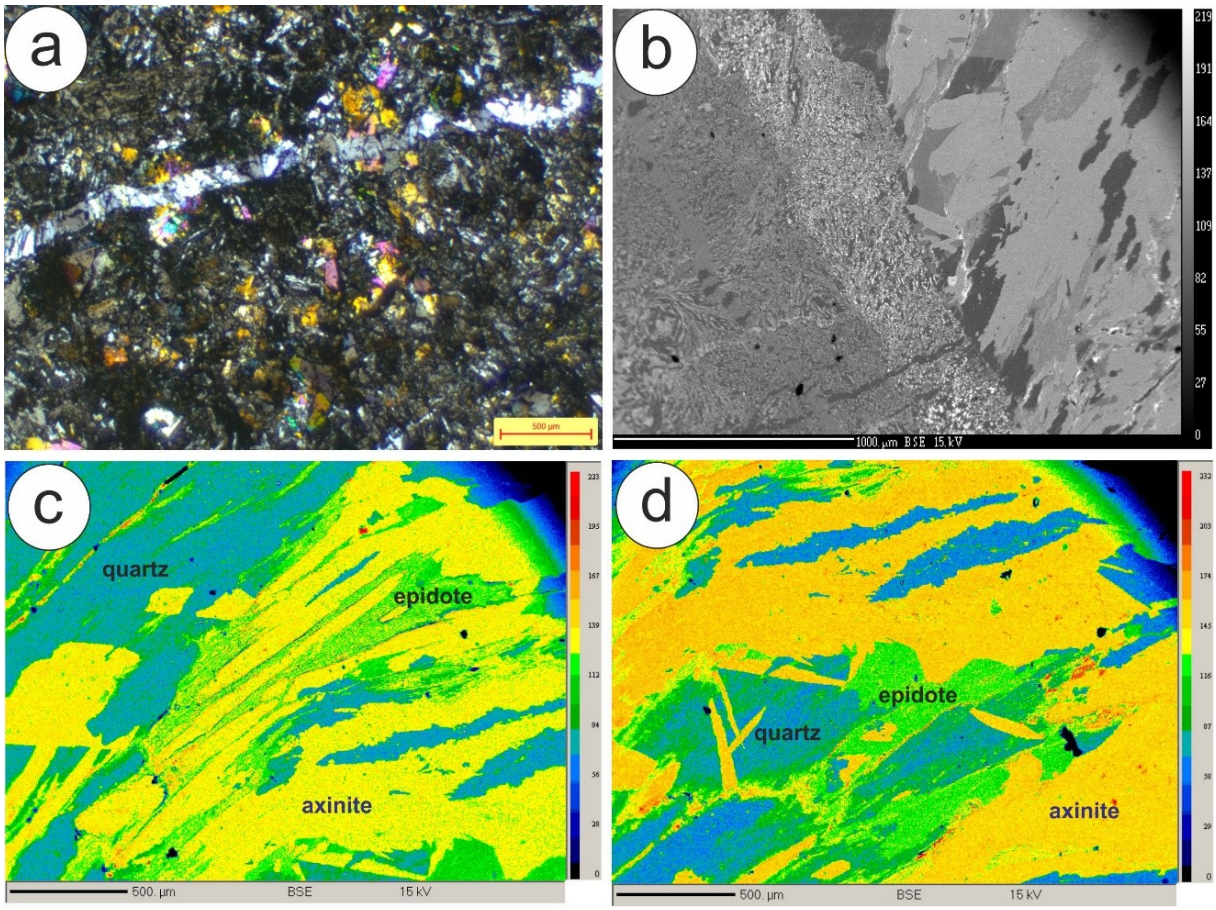

Fig. 4. a) Photomicrograph showing transverse of axinite vein within DKB volcanic, b) Backscattered Electron (BSE) image showing contact between Bijli rhyolite and axinite-quartz vein, c-d) False Colour Composite (FCC) images showing contact quartz-epidote association with rhombic to elongated shaped axinite.

for CO_2, N_2, and CH_4 analyses in the vapor phase was 500–4000 cm^{-1}. The Raman spectra were acquired for 10–50 s. The spectral resolution for each Raman vibrational mode is on the order of ±1 to 2 cm^{-1}.

4. Result

4.1. Petrography and Mineral Chemistry

The axinite in the quartz + axinite vein is observed as euhedral wedges or rhomboidal crystals developed from the wall of the host rock (Fig. 4a–b). They are devoid of zoning and show a single uniform distribution of elements (Fig. 4c–d). Epidote and chlorite are the principal alteration minerals associated with axinite. The axinite-quartz veins also contain disseminated sulphide mineralisation, mainly consisting of pyrite, chalcopyrite, pyrrhotite, and arsenopyrite, as well as the replacement of chalcopyrite to covellite and pyrrhotite to marcasite (Fig. 7a–d). The presence of tiny grains of gold was also observed along with a magnetite vein in the andesite (Fig. 7e).

It exhibits a common association with quartz, epidote, and chlorite, as supported by X-ray diffraction data (Fig. 5a). Backscattered Electron (BSE) images obtained using a Secondary Electron Microscope (SEM) also reveal the presence of euhedral wedges or rhomboidal crystals associated with other alteration phases. Representative major element chemical compositions of axinites are shown in Table 1. The SiO_2 and CaO contents range from 37.52 wt.% to 38.35 wt.% and from 22.77 wt.% to 24.19 wt.%, respectively. The average contents of FeO and Al_2O_3 in axinite are 8.46 wt.% to 10.88 wt.% and 23.73 wt.% to 25.45 wt.%, respectively. According to the FeO/(MnO + FeO) ratios is very high (0.97–1) and the MgO–MnO–FeO triangular diagram, axinites belong to the ferro-axinite (Fig. 5b).

4.2. Raman Spectroscopy of Fluid Inclusions

Quartz grains associated with axinite show both monophase and biphase fluid inclusions. The morphology of the inclusions is generally irregular,

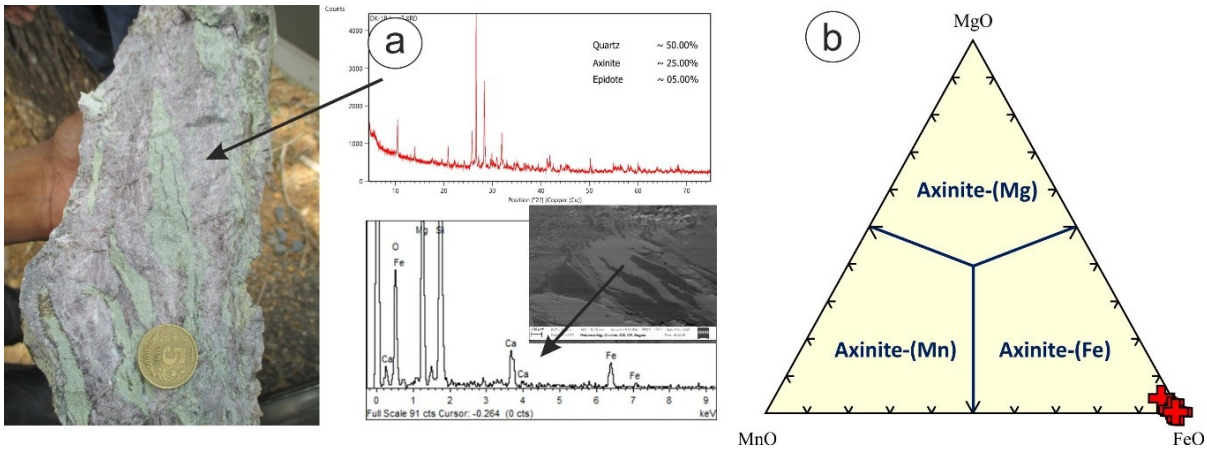

Fig. 5. a) Composite diagram showing purple-pink axinite sample with X-Ray Diffraction (XRD) and SEM-WDS spectra's, b) The MnO–MgO–FeO triangular diagram showing ferro-axinite nature of sample.

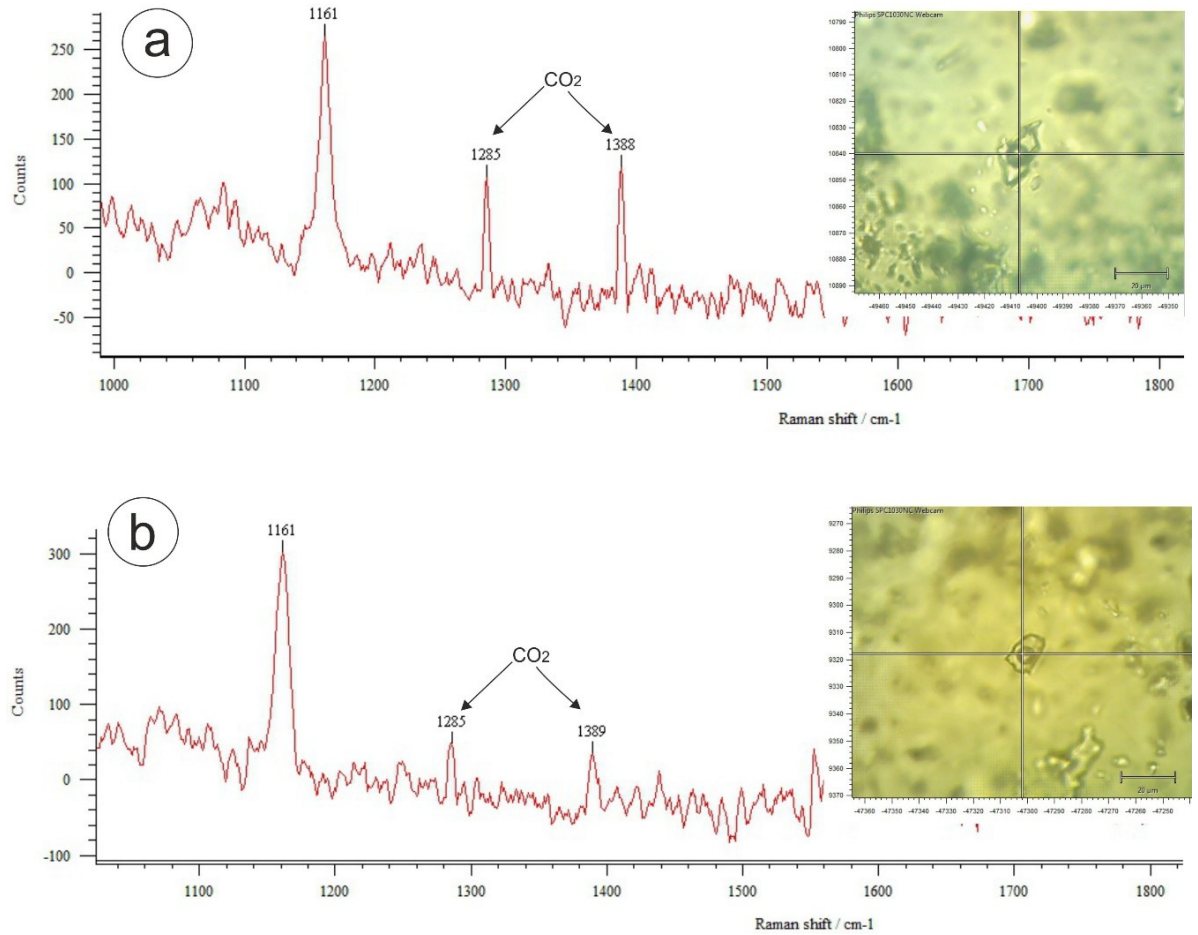

Fig. 6. a–b) Raman spectroscopy images showing presence of CO_2 peaks in the fluid inclusion within quartz-axinite veins.

facetted, sub-rounded, and oval, and the size of inclusions varies from 1 to 10 µm, inhomogeneously distributed throughout the sample. The inclusions furnish Raman peaks predominantly present of primary and pseudosecondary aqueous phases and Raman peaks at 1284 cm^{-1}, 1285 cm^{-1}, 1286 cm^{-1}, 1388 cm^{-1}, and 1389 cm^{-1} corresponding to pure CO_2 (Fig. 6a–b). Similarly, Raman peaks at 711 cm^{-1}, 714 cm^{-1}, and 715 cm^{-1} corresponding to axinite (Fig. 6c–d).

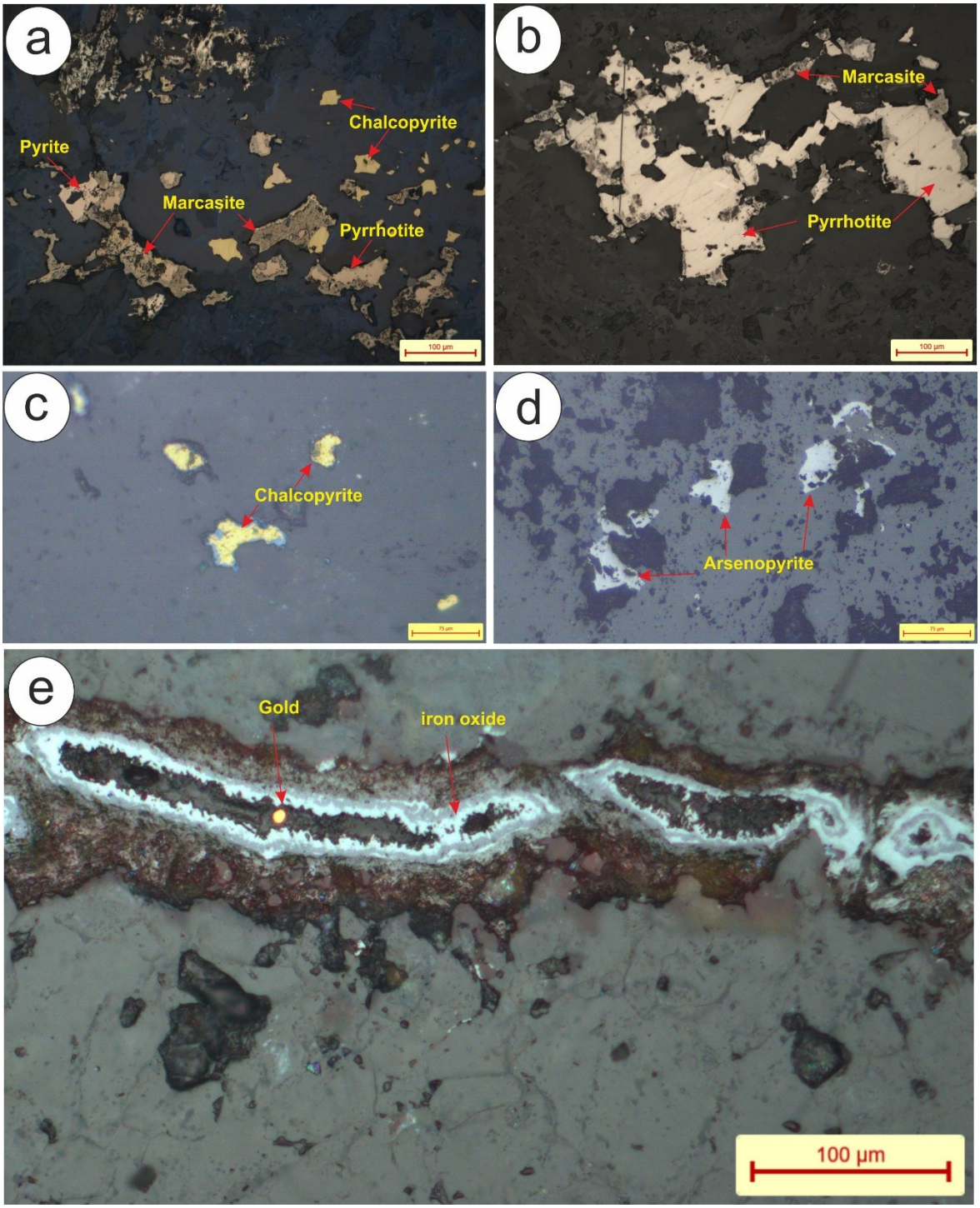

Fig. 7. a) photomicrograph showing the presence of pyrite, chalcopyrite, pyrrhotite and replacement of pyrrhotite to marcasite in the smoky quartz vein, b) photomicrograph showing the replacement of pyrrhotite to marcasite, c) photomicrograph showing the replacement of chalcopyrite to covellite, d) photomicrograph showing the presence of arsenopyrite in the smoky quartz vein, e) photomicrograph showing the tiny gold grain associated with iron oxide vein in the smoky quartz vein.

5. Discussion

5.1. Genesis of Axinite

The most characteristic skarn mineral was abundantly occurring axinite, which can be formed under a plentiful supply of boron derived from magma or a hydrothermal solution. Boron content is a good indicator for understanding the magmatic–hydrothermal evolutionary processes forming metallic deposits (Thomas et al., 2003). Axinite is the

most characteristic skarn mineral and occurs abundantly in various types of deposits (Chaudhry and Howie, 1969; Kurshakova, 1976; Grew, 1996; Karas and Pakhomova, 2012; Georgievskiy et al., 2019; Kim et al., 2021). Axinites occur mostly as large crystals with a wedge or axe-head shape, or sometimes a fragmented, irregular shape. They occur as cavity fillings and veinlets. Axinite replaces primary calcite and the retrograde skarn minerals, amphibole, and epidote (Kim et al., 2021). Boron is an incompatible element characteristically found in felsic melt and usually decreases with H_2O content. Mica can incorporate a significant amount of boron, so shale-type sedimentary rock and volcanics originating from the melting of such types of sediments can be rich in boron. Alternatively, smectites in the oceanic crust can absorb boron from seawater, or metamorphism can also lead to the depletion of boron due to devolatilization (Leeman and Sisson, 2018). The host Khairagarh metavolcanics, i.e., andesite and rhyolite, indicate a primitive mantle source with crustal influence in their genesis, or mafic volcanics in association with continentally derived sediments, which probably indicates back-arc rifting in an Andean-type subduction environment (Longjam and Ahmad, 2011; Asthana et al., 2014). Such mantle evolution processes generally lead to the boron metasomatism and formation of axinite and tourmaline in the mafic and felsic volcanic rocks (Leeman and Sisson, 2018; Balassa et al., 2023).

The regional active boron-rich hydrothermal system is evident in the Sakoli Fold Belt, with several occurrences of the most common borosilicate minerals, tourmaline and dumortierite, associated with Cu–Au–Pb–Zn mineralisation (Saha et al., 1996; Mishra et al., 2001; Biswas, 2002; Meshram and Ingle, 2012). Nevertheless, axinite is not yet reported from the vicinity Cu–Au–Pb–Zn prospect of the Sakoli fold belt or the Cu–Au mineralisation in the DKB. The present study shows control of axinite-quartz vein genesis along the contact of rhyolite-andesite with sandstone/conglomerate with a regional hydrothermal system that carries copper-gold mineralisation along the DKB. The predominance of axinite in the area rather than tourmaline supports a calcic-basic, Al-poor environment with very low temperature and pressure at low CO_2 fugacity (Hietanen and Erd, 1978; Pringle and Kawachi, 1980; Grew, 1996; Filip et al., 2006). Hietanen and Erd (1978) explain that axinite forms in a wider P–T range in different geological environments. Axinite generally forms in elevated pH conditions (Hayes et al., 2009; Zagorsky, 2015). Pringle and Kawachi (1980) suggested a miscibility gap in the axinite group at low temperatures, which might explain the scarcity of magnesioaxinite in nature. High miscibility in ferroan magnesioaxinite to magnesian ferroaxinite from originating at the temperature ~300 –400 °C, indicates that such a miscibility gap should occur at lower temperatures. Because of most axinites are formed at temperatures near 300 °C and higher (Grew, 1996 and references therein), immiscibility is unlikely to control the scarcity of magnesioaxinite (Novák and Brno, 2002). It is assumed that the axinite in the DKB derived boron primarily from the surrounding metavolcanic rocks, most likely from rhyolite, as suggested by evidence of boron metasomatism during its petrogenetic processes (Pringle and Kawachi, 1980; Fehér, 2015; Krmíček et al., 2021; Balassa et al., 2023). Additionally, boron may have been introduced through fault zones and fractures, controlled by hydrothermal fluids circulating within the host DKB metavolcanics. This supports a magmatic origin for the axinite, overprinted by hydrothermal activity. It is generally used as an indicator for understanding the magmatic–hydrothermal evolutionary processes that form metallic deposits (Thomas et al., 2003).

5.2. Implication for Sulphide-Gold Mineralisation

The common association of axinite-quartz vein with sulphide-gold bearing veins reveals their genetic link. The main sulphide minerals are pyrite, chalcopyrite, and pyrrhotite, which also show the replacement of pyrrhotite by marcasite and chalcopyrite by covellite, accompanied by the presence of tiny grains of gold. The different textures among pyrrhotite, pyrite, chalcopyrite and marcasite reflect the dominance of the crystal growth of marcasite as a precipitation mechanism from solution. Qian et al. (2011) experimental study suggested that the pyrrhotite to Fe disulphide reaction proceeds by a dissolution-reprecipitation mechanism under hydrothermal conditions, with a preference for low pH at temperatures below 220 °C. Schoonen and Barnes (1991b,c) experimental studies said that < 100ºC, pyrite, and marcasite are formed by sulfidation of amorphous FeS with polysulphides, and > 100ºC, pyrite and marcasite are formed via sulfidation and possibly through loss of iron out of FeS precursor phases (Schoonen and Barnes, 1991b,c).

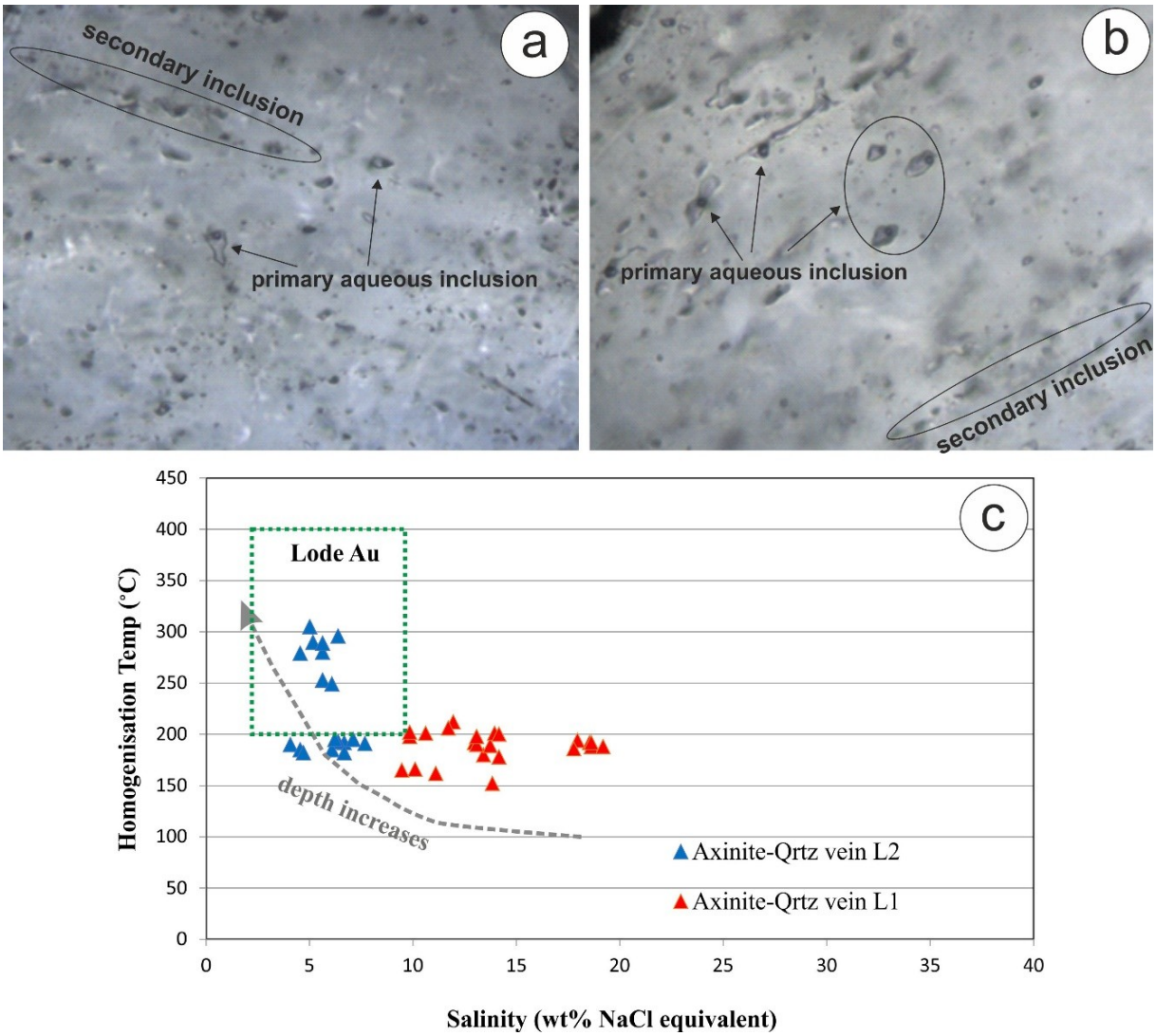

Fig. 8. a)–b) Fluid inclusions in axinite-quartz vein showing primary aqueous inclusions. c) Homogenization temperature (Thom) vs. salinity plots for fluid inclusions in axinite-quartz vein from the study area.

Both marcasite and pyrite are only stable in neutral to alkaline solutions below 240°C (Giggenbach, 1974; Schoonen, 1989). Formation of pyrite and marcasite under hydrothermal conditions is generally agreed that marcasite forms under acidic conditions (pH<5), or in S(-II)-deficient solutions while pyrite is formed at relatively higher pH or S(-II)-rich solutions (Murowchick and Barnes, 1986; Schoonen and Barnes, 1991b,c,a; Murowchick, 1992; Qian et al., 2011). The marcasite to pyrite transformation is extremely slow at below 300 °C, and marcasite can survive over geological time at below 300 °C (Fig. 7a–b) (Lennie and Vaughan, 1992; Murowchick, 1992; Yao et al., 2020). Several experiments have demonstrated that Au is hosted in sulphide minerals with the following decreasing order of Au concentration: bornite>chalcopyrite>pyrrhotite> pyrite (Fig. 7c–d) (Cygan and Candela, 1995; Jugo et al., 1999; Simon et al., 1999, 2000). Generally, cooling from 400 to 300 °C results in precipitation of 90% of the dissolved gold as metallic Au in quartz veins (Kerrich, 1999). Gold mostly concentrates in high-sulphidation systems at 300 °C at low pH (<2) and high log$f(O_2)$ (-28) (Archibald et al., 2001). It seems more likely that a decrease in pressure, combined with a drop in temperature below ~300 °C, would have been an important factor for gold precipitation, along with the brittle-ductile shear processes (Fig. 7e, 8c) (e.g., Zhu et al., 2007). The presence of an axinite-quartz vein with associated sulphide and gold mineralisation within the hydrothermal system along the brittle-ductile zones in the DKB suggests low-pressure, 300 °C temperature ranges for the precipitation of gold mineralisation (Fig. 8c).

e-ISSN: 2583-6900

Table 2. Representative Salinity and temperature homogenization data of fluid inclusion study from the ferro-axinite from quartz-axinite veins of the Dongargharh-Kotri Belt.

IncNum	IncType	Class	Te	Tm_ice	Ts_hal	Th_total	Tm_CO_2	Th_CO_2	Th_CH4	Phase	Tm_clathrat	EqWt%NaCl	Density
1	V+L	Primary	-23	-9.9		152				Liquid		13.8387	1.0163
2	V+L	Primary	-24	-9.5		180				Liquid		13.4077	0.988
3	V+L	Primary	-19	-10.2		178				Liquid		14.1559	0.9956
4	V+L	Primary	-28	-14.9		192				Liquid		18.5354	1.0173
5	V+L	Primary	-29	-15		188				Liquid		18.6183	1.0216
6	V+L	Primary	-27	-15.7		188				Liquid		19.1884	1.0262
7	V+L	Primary	-28	-9.8		189				Liquid		13.7319	0.982
8	V+L	Primary	-29	-9.1		192				Liquid		12.9669	0.9731
9	V+L	Primary	-28	-9.2		190				Liquid		13.0781	0.9759
10	V+L	Primary	-29	-15		192				Liquid		18.6183	1.0179
11	V+L	Primary	-30	-14.2		194				Liquid		17.9446	1.0106
12	V+L	Primary	-28	-14		186				Liquid		17.7723	1.0167
13	V+L	Primary	-29	-8.2		212				Liquid		11.9381	0.9448
14	V+L	Primary	-28	-7.1		201				Liquid		10.6065	0.9457
15	V+L	Primary	-29	-6.5		198				Liquid		9.8436	0.9429
16	V+L	Primary	-29	-10		201				Liquid		13.945	0.9719
17	V+L	Primary	-28	-8		206				Liquid		11.7023	0.9491
18	V+L	Primary	-29	-9.2		198				Liquid		13.0781	0.9681
19	V+L	Primary	-30	-10.2		200				Liquid		14.1559	0.9746
20	V+L	Primary	-28	-6.7		166				Liquid		10.1009	0.9762
21	V+L	Primary	-26	-6.2		165				Liquid		9.4522	0.9724
22	V+L	Primary	-27	-7.5		162				Liquid		11.1005	0.9871
23	V+L	Primary	-26	-6.5		202				Liquid		9.8436	0.9388
25	V+L	Primary	-26	-3.5		280				Liquid		5.6239	0.8021
25	V+L	Primary	-27	-3.2		290				Liquid		5.1657	0.7813
26	V+L	Primary	-26	-2.8		279				Liquid		4.5457	0.7922
27	V+L	Primary	-28	-2.5		190				Liquid		4.0743	0.9084
28	V+L	Primary	-29	-2.8		185				Liquid		4.5457	0.9172
29	V+L	Primary	-25	-2.9		182				Liquid		4.7017	0.9216
30	V+L	Primary	-28	-3.1		305				Liquid		5.0117	0.7544
31	V+L	Primary	-29	-3.5		253				Liquid		5.6239	0.8418
32	V+L	Primary	-24	-4.9		191				Liquid		7.6774	0.9338
33	V+L	Primary	-25	-4.2		192				Liquid		6.6686	0.9252
34	V+L	Primary	-28	-4.5		195				Liquid		7.1054	0.9253
35	V+L	Primary	-26	-4		193				Liquid		6.3737	0.922
36	V+L	Primary	-27	-3.8		249				Liquid		6.0759	0.8515
37	V+L	Primary	-24	-4.2		182				Liquid		6.6686	0.9357
38	V+L	Primary	-25	-3.8		185				Liquid		6.0759	0.9283
39	V+L	Primary	-26	-3.9		195				Liquid		6.2252	0.9187
40	V+L	Primary	-25	-4		296				Liquid		6.3737	0.7853
41	V+L	Primary	-26	-3.5		289				Liquid		5.6239	0.788

5.3. Significance of Fluid Inclusion and Raman Spectroscopy Study

The fluid characteristics from the quartz grain associated with axinite show the presence of dominant primary aqueous inclusions (vapour+liquid) along with the development of speudosecondary trails/tracks (Fig. 8a–b). These primary aqueous inclusions mainly contain moderate salinity ranges from 10 to 20 wt.% NaCl (Table 2). It shows restricted homogenization temperatures between 150 °C and 200 °C (Fig. 8c). In contrast, a few samples collected from lower elevation levels from the same axinite-quartz vein show the presence of CO_2-rich phases, as confirmed by Raman spectroscopy (Fig. 6), and have low salinity, ranging from 5 to 10 wt.% NaCl. It shows restricted homogenization temperatures between 170 °C and>300 °C (Fig. 8c). This suggests that carbonic phases with low salinity and homogenization temperatures between 200 °C and 400 °C generally indicate the precipitation of gold mineralisation in the hydrothermal system (Fig. 8) (Wilkinson, 2001). The inverse relationship between salinity and homogenisation temperature across sample locations indicates a change in the fluid regime from shallower to deeper levels, which favours gold mineralisation within the host axinite–quartz vein and supports its auriferous nature.

6. Conclusion

The presence of rare axinite (Fe) in the Dongargarh-Kotri Belt (DKB) and its association with sulphide gold occurrences is discussed first time. Ferro-axinite occurs in two different types i.e, as small veins/stringers within rhyolite-andesite as well as along the contact between volcanics and sedimentary rocks. Both magmatic-hydrothermal processes and associated boron metasomatism in the area control the genesis. The presence of axinite in DKB instead of tourmaline indicates limited carbonatization, with available Ca combined with B, Fe, and Si at very low hydrothermal temperatures. The presence of sulphides i.e, pyrite, chalcopyrite, arsenopyrite, pyrrhotite and marcasite in association with axinite indicates high sulphidation, at 300 °C and low pH (<5). The presence of primary aqueous and CO_2-rich phases with low to moderate salinity (5 to 20 wt.% NaCl) and restricted homogenization temperatures between 150 °C and >300 °C strongly supports its auriferous nature. It is further explained that the boron-rich hydrothermal system occurs in low-pressure, low-pH, and ~300 °C temperature ranges, favouring the precipitation of gold mineralisation along the brittle-ductile zones in the DKB. Furthermore, the present study suggests that the DKB gold prospects have no or limited occurrences of tourmaline and favour the spatiotemporal association of ferro-axinite with the sulphide gold mineralisation, revealing its indicator mineral or pathfinder nature.

Acknowledgement

The authors extend sincere thanks to the Additional Director General, Geological Survey of India, Central Region, for the permission to publish this work. The present work is the outcome of the Field Season program (2023–2024) of the Regional Petrology Division, GSI, CR Nagpur. The authors also extend their sincere gratitude to an anonymous reviewer for critical scrutiny and constructive suggestions, which immensely helped to improve the manuscript. Finally, the authors are thankful to the Chief Editor for providing an opportunity and kind consideration of our research in the journal. The authors extend their sincere gratitude to the Reviewers for their critical scrutiny and suggestions, which immensely helped to improve the manuscript.

Data availability statement

The authors confirm that the data supporting the findings of this study are available within the article [and/or] its supplementary materials.

CRediT statement

Author contributions: **TM:** project administration (lead), writing – original draft (lead); **TM, NR & RM**: conceptualization (lead); data curation (supporting), **LS, GM, DS, KKD, SC, RW, MLD, SB**: data curation (supporting), formal analysis (supporting), investigation (supporting).

Funding/Declaration

This research received no specific grant from any funding agency in the public, commercial, or not-for-profit sectors.

Competing Interests/Ethical statements

The authors declare that they have no known competing financial interests or personal relationships that could have appeared to influence the work reported in this paper.

References

Andreozzi, G.B., Lucchesi, S., Graziani, G., Russo, U., 2004. Site distribution of Fe2+ and Fe3+ in the axinite mineral group: New crystal-chemical formula. *American Mineralogist* 89, 1763–1771.

Archibald, S.M., Migdisov, A.A., Williams-Jones, A.E., 2001. The stability of Au-chloride complexes in water vapor at elevated temperatures and pressures. *Geochimica et Cosmochimica Acta* 65, 4413–4423.

Asthana, D., Pophare, A.M., Kumar, H., 2014. Dongargarh-Kotri Belt: An Intra-continental Rift or an Andean-Type Active Continental Margin Related Mobile Belt? *Gondwana Geological Magazine* 16, 215–218.

Balassa, C., Németh, N., Kristály, F., 2023. New Axinite Occurrence from Bükk Mts., NE Hungary. *Geosciences and Engineering* 11(1), 89–103.

Biswas, S.K., 2002. Gold deposits of India. *Indian Journal of Geology* 74(14), 187–207.

Bleeker, W., 2003. The late Archaean record: A puzzle in ca. 35 pieces. *Lithos* 71(2-4), 99–134.

Chaudhry, M.N., Howie, R.A., 1969. Axinites from the contact skarns of the Meldon aplite, Devonshire, England. *Mineralogical Magazine* 37, 45–48.

Cygan, G.L., Candela, P.A., 1995. Preliminary study of gold partitioning among pyrrhotite, pyrite, magnetite, and chalcopyrite in gold-saturated chloride solutions at 600° to 700 °C, 140 MPa (1400 bar), in: Thompson, J.F.H. (Ed.), Magmas, Fluid, and Ore Deposits, Short Course Series. Mineralogical Association of Canada, Ontario. volume 23, p. 129–137.

Deshpande, G.G., Mohabey, N.K., Deshmukh, M.S., 1990. *Petrography and tectonic setting of Dongargarh volcanic in Precambrian of central India.* volume 28. Geological Survey of India. Special Publication.

Fehér, B., 2015. Turmalin kötőanyagú hidrotermás breccsa Miskolc-Bükkszentlászlóról. *A Herman Ottó Múzeum Évkönyve* LIV, 11–23.

Filip, J., Kolitsch, U., Novák, M., Schneeweiss, O., 2006. The crystal structure of near-end-member ferroaxinite from an iron-contaminated pegmatite at Malesov, Czech Republic. *The Canadian Mineralogist* 44, 1159–1170.

Georgievskiy, A.F., Bugina, V.M., Rogova, O.Y.U., Georgievskiy, A.A., 2019. New data on mineral complexes of the Turgoyak limestone deposit (South Ural). *Materials Science and Engineering* https://doi.org/10.1088/1757-899X/675/1/012034.

Ghosh, J.G., Pillay, K.R., 2012. Evolution of the Kotri linear belt; a late Archaean continental rift in the Bastar Craton, Central India, in: National workshop on recent advances in geology of Dongarh-Kotri belt, central India and its mineral potential, Abstracts. AMD and Gondwana Geological Society Nagpur, p. 16–17.

Giggenbach, W.F., 1974. Equilibria involving polysulphide ions in aqueous solutions up to 240°C. *Inorganic Chemistry* 13, 1724–1730.

Govil, H., Mishra, G., Gill, N., Taloor, A., Diwan, P., 2021. Mapping Hydrothermally Altered Minerals and Gossans using Hyperspectral data in Eastern Kumaon Himalaya, India. *Applied Computing and Geosciences* https://doi.org/10.1016/j.acags.2021.100054.

Grew, E.S., 1996. Borosilicates (exclusive of tourmaline) and boron in rock-forming minerals in metamorphic environments. Chapter 9. *Reviews in Mineralogy & Geochemistry* 33, 387–502.

Hammarstrom, J.M., Zen, E., 1986. Alamosite and Axinite in Skarn Deposits of the Southwestern United States. *USGS Bulletin* , 1555URL: https://pubs.er.usgs.gov/publication/b1555.

Hayes, S.M., White, S.A., Thompson, T.L., Maier, R.M., Chorover, J., 2009. Changes in lead and zinc lability during weathering-induced acidification of desert mine tailings: Coupling chemical and micro-scale analyses. *Applied geochemistry: journal of the International Association of Geochemistry and Cosmochemistry* 42(12), 2234–2245.

Hietanen, A., Erd, R.C., 1978. Ferroaxinites from the Feather River area, northern California, and from the McGrath and Russian Mission quadrangles, Alaska | U.S. Geological Survey. *Journal of Research of the U.S. Geological Survey* 6(5), 603–610.

Jugo, P.J., Candela, P.A., Piccoli, P.M., 1999. Magmatic sulphide s and Au: Cu ratios in porphyry deposits: an experimental study of copper and gold partitioning at 850 °C, 100 MPa in a haplogranitic melt-pyrrhotite-intermediate solid solution-gold metal assemblage, at gas saturation. *Lithos* 46, 573–589.

Karas, O.A., Pakhomova, V.A., 2012. Fluid regime of the Dalnegorsk boron-rich lime-skarn deposit f rm ti n (the Primorsky Region, Russia). *Zapiski RMO (Proceedings of the Russian Mineralogical Society)* 6, 18–28. In Russian.

Kerrich, R., 1999. Nature's gold factory. *Science* 284, 2101–2102.

Kim, N., Koh, S.M., You, B.W., Lee, B.H., 2021. Mineralogy, Geochemistry, and Age Constraints on the Axinite-Bearing Gukjeon Pb–Zn Skarn Deposit in the Miryang Area, South Korea. *Minerals* 11, 619.

Kowal-Linka, M., Rychła, A., 2022. Mineralogical and Geochemical Indicators of Boron Metasomatism in Skarn Systems. *Minerals* 12(1), 93. https://doi.org/10.3390/min12010093.

Krishnamurthy, P., Sinha, D.K., Rai, A.K., Seth, D.K., Singh, S.N., 1990. *Magmatic rocks of the Dongargarh Supergroup – their petrological evolution and implications on metallogeny.* volume 28. Geological Survey of India Special Publication.

Krmíček, L., Novák, M., Trumbull, R.B., Cempírek, J., Houzar, S., 2021. Boron isotopic variations in tourmaline from metacarbonates and associated calc-silicate rocks from the Bohemian Massif: Constraints on boron recycling in the Variscan orogen. *Geoscience Frontiers* 12(1), 219–230.

Kurshakova, L.D., 1976. Physico-chemical conditions of skarn-borosilicate deposits. In Russian.

Leeman, W.P., Sisson, V.B., 2018. Geochemistry of boron and its implications for crustal and mantle processes. Chapter 12. *Reviews in Mineralogy & Geochemistry* 33, 645–708.

Lennie, A.R., Vaughan, D.J., 1992. Kinetics of the marcasite-pyrite transformation; an infrared spectroscopic study. *American Mineralogist* 77, 1166–1171.

Longjam, K.C., Ahmad, T., 2011. Geochemical characterization and petrogenesis of Proterozoic Khairagarh volcanics: implication for Precambrian crustal evolution. *Geological Journal* https://doi.org/10.1002/gj.1312.

Meshram, R.R., Ingle, K.B., 2012. Mineralogy and Origin of Dumortierite from Girola Area, Bhandara District, Eastern Maharashtra. *Journal Geological Society of India* 79, 181–188.

Mishra, H., Saha, G., Jena, S.K., Patel, M.K., Patel, M.C., 2012. Geological Characteristics and Nature of Gold Mineralisation in the Sonadehi area, Kotri belt, Kanker District, Chhattisgarh, in: National workshop on recent advances in geology of Dongarh-kotri belt, central India and its mineral potential, Abstracts. AMD and Gondwana Geological Society Nagpur, p. 16–17.

Mishra, T., Jose, B., Deepa, K.K., Sreehari, S.M.S., Venkatesh, A.S., 2001. Auriferous mineralisation in the Sakoli Group, central India, with particular reference to sulphide-bound gold. *Applied Earth Science* 110(2), 103–109.

Mishra, V.P., Dutta, N.K., 2012. Precambrian Volcanism and Metallogeny in Kotri Belt, Bastar Craton, Chhattisgarh, India, in: National workshop on recent advances in geology of Dongarh-kotri belt, central India and its mineral potential, Abstracts. AMD and Gondwana Geological Society Nagpur, p. 16–17.

Murowchick, J.B., 1992. Marcasite inversion and the petrographic determination of pyrite ancestry. *Economic Geology* 87(4), 1141–1152.

Murowchick, J.B., Barnes, H.L., 1986. Marcasite precipitation from hydrothermal solutions. *Geochim. Cosmochim. Acta* 50, 2615–2630.

Naqvi, S.M., 2005. *Geology and Evolution of the Indian Plate*. Capital Publishing Co, New Delhi.

Neogi, S., Miura, H., Hariya, Y., 1996. Geochemistry of the Dongargarh volcanic rocks, Central India: implications for the Precambrian mantle. *Precambrian Research* 76, 77–91.

Novák, M., Brno, J.F., 2002. Ferroan magnesioaxinite from hydrothermal veins at Lazany, Brno Batholith, Czech Republic. *N. Jb.Miner. Mh* 9, 385–399.

Pouchou, J.L., Pichoir, F., 1984. New model for quantitative x-ray microanalysis. Part I: Application to the analysis of homogeneous samples [English Ed.], in: Recherche Aerospatiale (English Edition). volume 3, p. 13–38.

Pringle, I.J., Kawachi, Y., 1980. Axinite mineral group in low-grade regionally metamorphosed rocks in southern New Zealand. *American Mineralogist* 65, 1119–1129.

Qian, G., Xia, F., Brugger, J., Skinner, W.M., Bei, J., Chen, G., Pring, A., 2011. Replacement of pyrrhotite by pyrite and marcasite under hydrothermal conditions up to 220 °C: An experimental study of reaction textures and mechanisms. *American Mineralogist* 96, 1878–1893.

Ramachandra, H.M., Roy, A., 1998. Geology of intrusive granitoids with particular reference to Dongargarh Granite and their impact on Tectonic Evolution of the Precambrian in Central India. *Indian Minerals* 52(1 and 2), 15–32.

Ramachandra, H.M., Roy, A., 2012. A Review of Evolutionary Characteristics of the Bastar Craton, in: National workshop on recent advances in geology of Dongarh-kotri belt, central India and its mineral potential, Abstracts. AMD and Gondwana Geological Society Nagpur, p. 16–17.

Ramakrishnan, M., Vaidyanadhan, R., 2010. *Geology of India*. volume 1. Geological Society of India, Bangalore.

Roy, A., Ramachandra, H.M., 2012. Emplacement of Neoarchaean-Palaeoproterozoic Granitoids in Dongargarh-Kotri Intra-cratonic Rift Zone: Implications for Crustal Growth and Evolution of Bastar Craton in Central India, in: National workshop on recent advances in geology of Dongarh-kotri belt, central India and its mineral potential, Abstracts. AMD and Gondwana Geological Society Nagpur, p. 16–17.

Roy, A., Ramachandra, H.M., Bandyopadhyay, B.K., 2000. *Supracrustal belts and their significance in the crustal evolution of central India*. volume I. Geological Survey India Special Publication.

Saha, A.K., Sashidharan, K., Padhi, R.N., Bhoskar, K.G., 1996. *Gold Mineralisation in Sakoli Supracrustals of Central Indian Shield, Maharashtra*. Mineral and Groundwater Resources of Vidarbha.

Saha, G., Mishra, H., Deb, S.K., Ashok Kumar, M.R., Patel, M.K., Shriramamurty, A., 2012. Geology and Nature of Gold Mineralisation in the Gurwandi area, Kotri belt, Chhattisgarh, in: National workshop on recent advances in geology of Dongarh-kotri belt, central India and its mineral potential, Abstracts. AMD and Gondwana Geological Society Nagpur, p. 16–17.

Sarkar, S.N., Gopalan, K., Trivedi, JR, 1981. New data on the geochronology of the Precambrian of Bhandara–Durg, Central India. *Indian Journal of Earth Science* 8, 131–151.

Sarkar, S.N., Sarkar, S.S., Ray, S.L., 1994. Geochemistry and genesis of the Dongargarh Supergroup Precambrian rocks in Bhandara–Durg Region, central India. *Indian Journal of Earth Science* 21, 117–126.

Schoonen, M.A.A., 1989. Mechanisms of pyrite and marcasite formation from solutions between 25 and 300°C. Ph.d. dissertation,. Pennsylvania State University.

Schoonen, M.A.A., Barnes, H.L., 1991a. Mechanisms of pyrite and marcasite formation from solution: III. *Hydrothermal processes. Geochimca et Cosmochimica Acta* 55, 3491–3504.

Schoonen, M.A.A., Barnes, H.L., 1991b. Reactions forming pyrite and marcasite from solution: I Nucleation of FeS2 below 100°C. *Geochim. Cosmochim. Acta* 55, 1495–1504.

Schoonen, M.A.A., Barnes, H.L., 1991c. Reactions forming pyrite and marcasite from solution: II. Via FeS precursor below 100 °C. *Geochimica et Cosmochimica Acta* 55, 1505–1514.

Sensarma, S., Mukhopadhyay, D., 2003. New Insight on the stratigraphy and volcanic history of the Dongargarh Belt, central India. *Gondwana Geological Magazine* 7, 129–136.

Shcheka, S.A., Bortnikov, N.S., Chernyshov, S.M., 2023. Mineral Formation in the Dalnegorsk Hydrothermal System, Russian Far East. *Crystals* 13(5), 743. https://doi.org/10.3390/cryst13050743.

Simon, G., Kesler, S.E., Chryssoulis, S., 1999. Geochemistry and textures of gold-bearing arsenian pyrite, Twin Creeks, Nevada; implications for deposition of gold in Carlin-type deposits. *Economic Geology* 94(3), 405–421.

Simon, G., Kesler, S.E., Essene, E.J., 2000. Gold in porphyry copper deposits: experimental determination of the distribution of gold in the Cu-Fe-S system at 400° to 700 °C. *Economic Geology* 95, 259–270.

Thomas, R., Heinrich, W., Förster, H.J., 2003. The behaviour of boron in peraluminous granite-pegmatite systems and associated hydrothermal solutions: A melt and fluid inclusion study. *Contribution to Mineralogy and Petrology* 144, 457–472.

Wilkinson, J., 2001. Fluid inclusions in hydrothermal ore deposits. *Lithos* 55, 229–272.

Yao, X., Xia, F., Deditius, A.P., Brugger, J., Etschmann, B.E., Pearce, M.A., Pring, A., 2020. The mechanism and kinetics of the transformation from marcasite to pyrite: in situ and ex-situ experiments and geological implications. *Contributions to Mineralogy and Petrology* 175(3), 1–25.

Zagorsky, V.Y.E., 2015. Sosedka pegmatite body at the Malkhan deposit of gem tourmaline, Transbaikalia: Composition, inner structure, and petrogenesis. *Petrology* 23(1), 68–92.

Zhu, Y.F., Zhou, J., Zeng, Y.S., 2007. The Tianger (Bingdaban) shear zone hosted gold deposit, west Tianshan, NW China: petrographic and geochemical characteristics. *Ore Geology Reviews* 32, 337–365.

